Experimental determination of dynamic crack initiation and propagation fracture toughness in thin aluminum sheets

D.M. OWEN, S. ZHUANG, A.J. ROSAKIS and G. RAVICHANDRAN
Graduate Aeronautical Laboratories, California Institute of Technology, Pasadena, California 91125, USA

Abstract. An experimental investigation was undertaken to characterize the dynamic fracture characteristics of 2024-T3 aluminum thin sheets ranging in thickness from 1.63–2.54 mm. Specifically, the critical dynamic stress intensity factor K_c^d was determined over a wide range of loading rates (expressed as the time rate of change of the stress intensity factor $\dot{K}_I^d$) using both a servo-hydraulic loading frame and a split Hopkinson bar in tension. In addition, the dynamic crack propagation toughness, K_D, was measured as a function of crack tip speed using high sensitivity strain gages. A dramatic increase in both K_c^d and K_D was observed with increasing loading rate and crack tip speed, respectively. These relations were found to be independent of specimen thickness over the range of 1.5 to 2.5 mm.

**Key words:** Fracture, dynamic crack initiation, thin aluminum.

1. Introduction

Extensive structural damage in commercial aircraft may occur over very short times as a result of high rate explosive loading. The macroscopic loading rates associated with such events have been estimated to be as high as $50 \times 10^6 \, \mathrm{N\,s^{-1}}$ (Kamoulakos, Chen, Mestreau & Lohner, 1996) with corresponding local strain rates on the order of $10^6 - 10^7 \, \mathrm{s^{-1}}$ (Meyers, 1994). The aircraft fuselage is typically fabricated using thin aluminum alloy sheets which are fastened to longitudinal stringers with rivets. Cracks may readily initiate from stress concentrations, such as rivet holes, in the vicinity of a blast, and subsequently travel at velocities on the order of a few hundred meters per second. These cracks can be driven by inertia and cabin pressure long after the dissipation of the explosion and may consequently travel substantial distances from the blast site leading to catastrophic structural failure.

In aging aircraft this scenario is even more probable, since these structures often possess widespread multisite fatigue damage in the form of aligned cracks emanating from rivet holes (Kanninen and O'Donoghue, 1995) as shown in Figure 1. The pre-existing fatigue cracks, if oriented favorably with respect to the stress waves generated by the blast, may initiate even in areas of the structure far from the blast site. Furthermore, the resulting dynamic cracks may travel with speeds as high as 60–70 percent of the decompression wave speed, c_D, in air ($c_D \sim 300 \, \mathrm{m\,s^{-1}}$). Under such conditions, as in the case of a pressurized pipeline, the driving force on the moving crack faces may be kept at sufficient levels (more than 50 percent of the cabin pressure) to propagate the cracks for distances much longer than current specifications allow, e.g. longer than 1–2 panels.

Figure 2 shows examples of such widespread damage in aircraft structures. Figure 2(a) is a photograph taken following a bomb blast experiment performed on a decommissioned B-52 aircraft (Barnes and Peters, 1992). Even in the absence of cabin pressure, dynamic cracks are
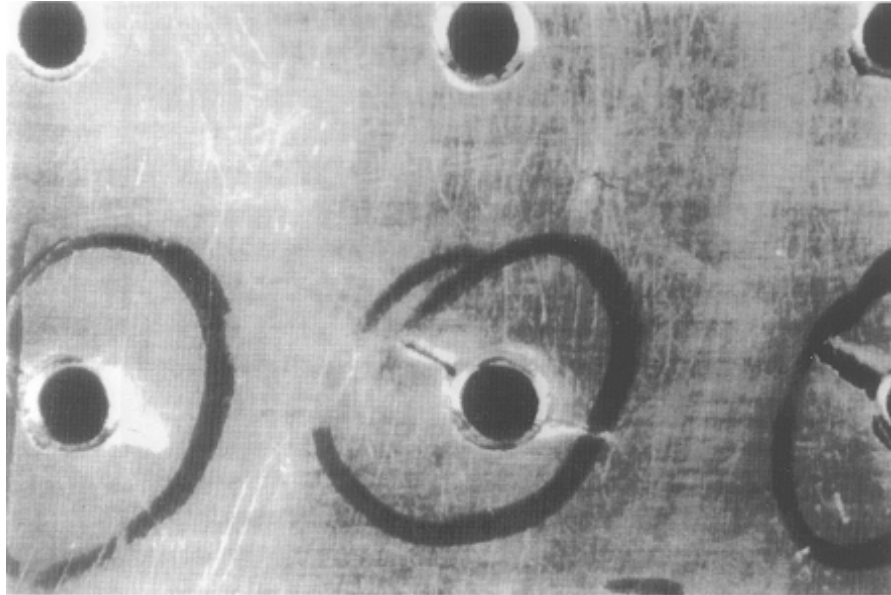
Figure 1. View of cracks emanating from a row of rivet holes – multisite damage (Kanninen and O'Donoghue, 1995).
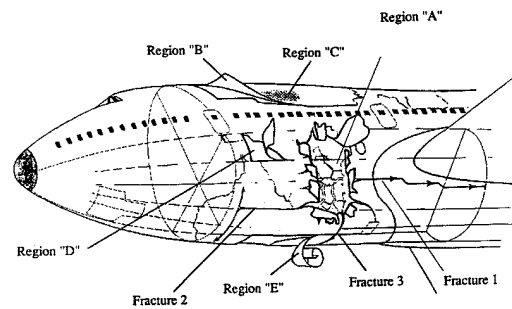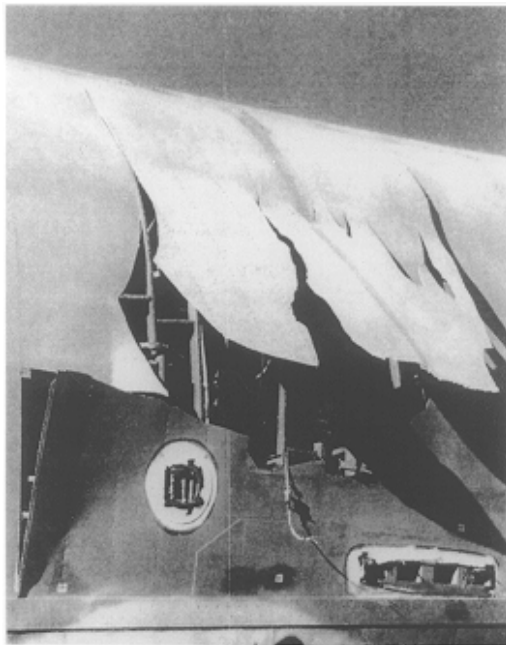
Figure 2. (a) Damage in a decommissioned B-52 aircraft resulting from a controlled experiment (Barnes and Peters, 1992). (b) Schematic illustration of explosive damage in Pan Am aircraft from the Lockerbie tragedy (UK Accidents Investigation Branch 1990).

seen to have propagated substantial distances from the blast site. Figure 2(b) is a schematic illustration which reconstructs the damage which occurred during the 1989 Pan Am tragedy in Lockerbie, Scotland (UK Accidents Investigation Branch 1990). Here damage is shown to have propagated both from the primary blast hole region and from other locations in the aircraft loaded by traveling stress waves (Kanninen and O'Donoghue, 1995).

One design strategy employed to induce crack arrest in aircraft structures involves the incorporation of tear straps. The implementation of tear straps in design practice relies typically on empirically based criteria. Recent analytical, numerical and experimental work by Kosai, Kobayashi and co-workers (Kosai and Kobayashi, 1991; Shimamoto, Kosai and Kobayashi, 1994; Kosai, Shimamoto, Yu, Kobayashi and Tan, 1996) has addressed issues relating to the effectiveness of tear straps in inducing crack arrest by considering the occurrence of crack kinking and crack flapping. However, these investigations have dealt strictly with relatively slow crack growth ($v \leqslant 20\,\mathrm{m\,s^{-1}}$) and does not represent conditions present during bomb blast events.

The failure processes associated with bomb blast events are transient and highly dynamic phenomena, featuring material separation at very high strain rates. Therefore, in order to predict the complex structural response and accumulation of damage in the aircraft resulting from an explosive blast, it is necessary to understand the fundamental constitutive and fracture behavior of aluminum sheets under high rate, dynamic loading. It is only through such understanding and characterization that aircraft design may be improved to minimize damage occurring as a result of explosions.

The distinct dynamic fracture regimes of initiation and growth are very important in transient events. First is the dynamic initiation of cracks, or the onset of dynamic crack growth. It has long been recognized in the literature (Freund, 1990; Freund, Duffy and Rosakis, 1981) that the initiation fracture toughness of structural metals is highly dependent on the rate of loading and may, in certain materials, be drastically different from the initiation fracture toughness obtained from quasistatic experiments. Thus in general, the crack initiation toughness is a material dependent function of loading rate. The second regime of interest is that of dynamic crack growth itself and subsequent arrest. The toughness of a dynamically growing crack in a particular material is often a strong function of crack tip velocity because it determines the local strain rate in the region directly ahead of the propagating crack. The dependence of toughness on crack tip velocity for a given material also dictates the conditions for crack arrest, such as maximum crack arrest lengths (Freund and Clifton, 1974; Freund, Duffy and Rosakis, 1981; Rosakis, Duffy and Freund, 1984; Freund, 1990).

Previous investigations of dynamic crack initiation over a wide range of loading rates have concentrated on the fracture characterization of polymeric materials. By using an electromagnetic loading device and the optical method of caustics in transmission, Ravi-Chandar and Knauss (1984) studied this phenomenon in Homalite-100. More recently, Rittel and Maigre (1995, 1996a, 1996b) used a modified Hopkinson bar technique to study dynamic crack initiation in PMMA by means of a novel hybrid analytical/experimental procedure. For structural metals, Wilson, Hawley and Duffy (1980) have presented extensive data for two distinct loading rates while varying the temperature over a wide range. In this study, a circumferentially notched round bar geometry was loaded explosively and toughness measurements were performed by means of an optical measurement of the critical crack opening displacement at initiation. This study, which also involved extensive micromechanical analysis of the resulting failure surfaces, clearly indicates the effect of loading rate on the Nil Ductility Temperature, NDT. An extensive discussion of the first (Ravi-Chandar and Knauss, 1984) and last (Wilson,

Hawley and Duffy, 1980) of these studies can be found in Chapter 3.6 of Freund's book on dynamic fracture mechanics (Freund, 1990).

Even fewer experimental investigations have been performed which address dynamic crack growth in structural solids. Two of the first studies of this nature were conducted by Rosakis, Duffy and Freund (1984) and Zehnder and Rosakis (1990) who examined highly dynamic crack growth in thick plates of AISI 4340 steel using the optical method of caustics in reflection in conjunction with high speed photography. The results indicated a very strong dependence of fracture toughness on crack tip speed, similar in nature to the equivalent relationship in polymers. Most of the prior research on dynamic crack growth has been performed on polymers using dynamic photoelasticity and this work has been discussed in Dally (1979).

This report describes the results of an experimental investigation into the dynamic fracture processes in 2024-T3 aluminum sheets. Specifically, the effect of loading rate (expressed as the time rate of change of the stress intensity factor) on the initiation fracture toughness, and the effect crack tip velocity on crack propagation toughness were determined in aluminum sheets ranging in thickness from 1.5–2.5 mm.

2. Background

It has long been recognized in the scientific community that the two dimensional near-tip deformation fields (plane strain or plane stress) in the vicinity of dynamically loaded cracks have a universal character whether they are stationary or propagating. The magnitude of this field is controlled by a time-dependent scalar, the dynamic stress intensity factor. As stated by Freund and Clifton (1974), the stress field with reference to a Cartesian coordinate system moving with the crack tip of 'all plane elastodynamic solutions for arbitrarily curving and propagating cracks of instantaneous length $a(t)$, can be asymptotically described by the following expression'

$$\sigma_{\alpha\beta} = \frac{K_{\mathrm{I}}^d(t)}{\sqrt{2\pi r}} f_{\alpha\beta}(\theta, \dot{a}(t)) + \mathrm{O}(l) \quad \text{as } r \to 0. \tag{1}$$

Here, (r, θ) is a polar coordinate system traveling with the crack tip, $f_{\alpha\beta}(\theta, \dot{a}(t))$ is a known universal function of time and crack tip speed $a(t)$. K_{I}^d is called the dynamic stress intensity factor. For stationary cracks under static loading $\dot{a}(t) = 0$; $K_{\mathrm{I}}^d(t) = K_{\mathrm{I}}^s$ where K_{I}^s is the static stress intensity factor. For stationary cracks that are dynamically loaded, e.g. by means of stress waves, $\dot{a} = 0$, however the amplitude K_{I}^d of the asymptotic stress field remains time varying and is still called the dynamic stress intensity factor

$$\sigma_{\alpha\beta} = \frac{K_{\mathrm{I}}^d(t)}{\sqrt{2\pi r}} f_{\alpha\beta}(\theta, 0) + \mathrm{O}(l) \quad \text{as } r \to 0. \tag{2}$$

It is also known that for more realistic materials, where the near crack tip region develops a *contained* active plastic zone, relation (1) will still hold in the elastic region surrounding the zone of contained plasticity. This active plastic zone is time varying for stationary dynamically loaded cracks and is also translating with the crack tip for moving cracks. In such a case, the dynamic stress intensity factor also characterizes the fracture process and determines the size and shape of the active plastic zone. This situation is often referred to as a condition of 'small scale yielding' (Freund, 1990). Small scale yielding (S.S.Y.) has experimentally been found

to accurately approximate fracture events in many high strength metals such as most steels, aluminum, and titanium alloys used in engineering practice. As a result, dynamic fracture criteria, even if local contained plasticity is present, can still be simply formulated by means of parameters such as the dynamic stress intensity factor.

If the initiation time and motion history of a crack tip is specified, the mechanical fields around it (and thus the instantaneous values of the stress intensity factors in (1)) can be obtained in principle within the context of linear elastic continuum mechanics as long as the configuration of the body and the details of time-dependent loading are also specified. This is often achieved numerically by means of the finite element method. However, since the initiation and motion of the crack tip is controlled completely by the transient deformation state and the micromechanics of separation of the surrounding material, the motion of the crack tip should not be specified a priori. Due to the fact that the constitutive equation for the material does not include the possibility of material separation, a mathematical statement of a crack growth criterion must be added to the governing equations. Such a criterion must be stated as a physical postulate on material behavior. This criterion should be at the same level as the kinematical theorems governing deformation, momentum balance principles, as well as the constitutive relation describing material response. The most common form for such a criterion is the requirement that the crack must initiate and then continue to grow at a particular crack tip speed in such a way that some parameter defined as part of the crack tip field maintains a certain critical level.

The critical level is specific to the material, temperature and local strain rate experienced at the crack tip, where the decohesion process takes place. For dynamically loaded stationary cracks, the near-tip strain rate and thus this critical level should depend on the resulting crack face opening rate just before crack initiation. For growing cracks the near-tip strain rate is related to the instantaneous crack tip speed. The resulting critical level of dynamic stress intensity factor sustainable by the material at a particular loading rate (stationary cracks) or necessary for crack advance at a particular crack tip speed (propagating cracks) is called the dynamic initiation or dynamic crack growth fracture toughness of the material, respectively. These critical levels and their dependence on rate, temperature or speed can only be determined through experimental measurements.

2.1. DYNAMIC INITIATION AT DIFFERENT LOADING RATES (THE DYNAMIC INITIATION CRITERION)

It has been observed experimentally that growth initiation of a stationary crack or flaw of length a_o at time $t = t_o$, occurs when the instantaneous value of the stress intensity factor $K_c^d(t)$ at $t = t_o$ ($\dot{a}(t) = 0$, $a = a_o$) reaches a critical value which is dependent on the material. In addition, this critical value also depends on the local, near-tip strain rate. A measure of this rate for small scale yielding is the time rate of change of the stress intensity factor (i.e. $\dot{K}_I^d$) (Freund, Duffy and Rosakis, 1981; Freund, 1990). This dependence reflects the local nonlinear deformation processes at the crack tip which generally are rate dependent, such as a rate dependent yield stress (strain rate hardening), and/or local thermal softening due to the adiabatic conversion of plastic work into heat. For ductile solids it also reflects the rate dependent process of void nucleation, growth and coalescence responsible for eventual crack extension. Given the above, the dynamic crack initiation criterion takes the form

$$K_I^d(P(t), a_o) = K_{IC}^d(\dot{K}_I^d(t)) \quad \text{at } t = t_o. \tag{3}$$

In the above equation, the left-hand side is the instantaneous value of the dynamic stress intensity factor, symbolically represented as a function of some generalized transient load $P(t)$. Alternatively, the right-hand side represents the critical value for initiation and is a material and temperature dependent function of loading rate, which is represented as $\dot{K}_I^d(t) = dK_I^d/dt$. The left-hand side is calculated using numerical techniques modeling the specific geometry and transient loading, whereas the right-hand side can only be determined experimentally for a specific material. The experimental measurement as a function of loading rate is best achieved in an arrangement which can provide a wide range of loading rates and a well-characterized loading history. Once the right-hand side has been obtained experimentally, (3) will provide the time of initiation and the level of stress intensity factor at that instant. For a particular boundary value problem it will also provide the maximum amplitude of the time varying loads at which crack growth will commence. For analytical examples of the left hand side of (3), see Freund (1990).

2.2.   CRACK TIP EQUATION OF MOTION (THE DYNAMIC CRACK GROWTH CRITERION)

When a crack begins to propagate, the fracture criterion has to be modified to take into account material inertia and rate effects resulting at the crack tip. In this case the material resistance to crack growth should depend on the near-tip strain rate through the crack tip velocity. This is customarily achieved as described below (Rosakis, Duffy and Freund, 1984; Zehnder and Rosakis, 1990; Freund, 1990).

Under general small scale yielding conditions, the dynamic solution (analytical or numerical) of a particular initial-boundary value problem will allow expression of the dynamic stress intensity factor as a function of generalized time dependent crack length $a(t)$ (reflecting the time evolving geometry), crack tip velocity $\dot{a}(t)$ (reflecting dynamic effects), time (reflecting the reflection of waves from geometrical boundaries, etc.), and a generalized load $P(t)$. As a result, we have that

$$K_I^d = K_I^d(P(t), a(t), \dot{a}(t), t). \tag{4}$$

Of course, as stated above, $a(t)$ and $\dot{a}(t)$ are not known a priori before some criterion is specified. The crack growth criterion states that for all times $t > t_o$, and $a(t) > a_o$, the crack will choose a crack length history $a(t)$ and a corresponding velocity history $\dot{a}(t)$, such that the instantaneous value of the dynamic stress intensity factor equals a quantity K_{ID}, called the dynamic crack growth toughness of the material, i.e.,

$$K_I^d(P(t), a(t), \dot{a}(t), t) = K_{ID}(\dot{a}(t)) \quad \text{for } t > t_o. \tag{5}$$

K_{ID} is a material dependent quantity, which has been found to depend on material properties, crack tip velocity (Rosakis, Duffy and Freund, 1984; Zehnder and Rosakis, 1990; Freund, 1990) and may also depend on temperature. The functional form of the left-hand side of (5) is completely determined by an elasticity solution (analytical or numerical, depending on the complexity of the problem). A number of analytical expressions for K_I^d for specific geometries, time dependent loading and general velocity histories are given by Freund (1990). However for most practical applications, $K_I^d(t)$ can only be obtained numerically. The right-hand side is called the dynamic crack growth toughness of the material. Its functional dependence has to be determined experimentally. Equation (4) is a non-linear, first order differential equation for $a(t)$, the crack length history. It is called the crack tip equation of
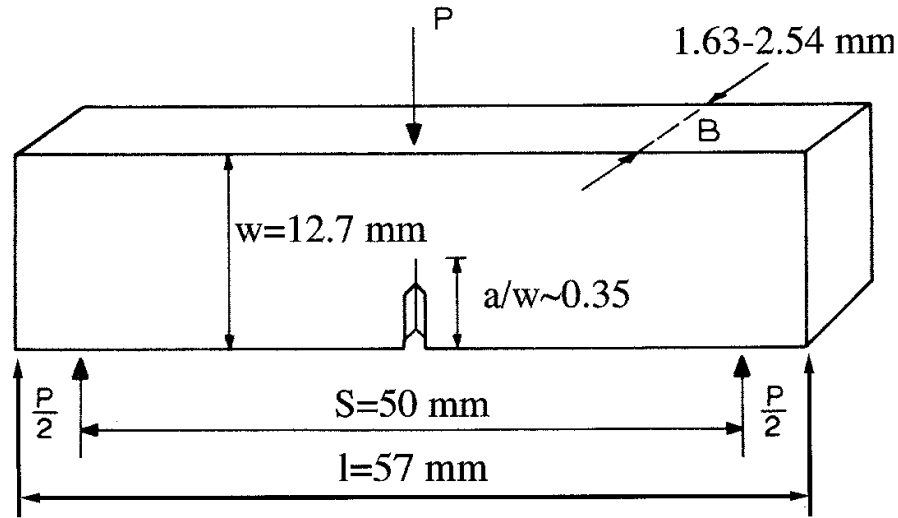
Figure 3. Schematic illustration of specimen geometry used in the experiments to determine K_c^d in the 3-point bend configuration used for fatigue and quasistatic testing.

motion. Once the right-hand side is determined for a specific material the above equation furnishes crack tip motion histories (including crack arrest) for any given geometry or loading. The velocity dependence of K_{ID} accounts for the interplay between plasticity, inertia and rate sensitivity in the dynamic material separation process.

2.3. EFFECT OF SPECIMEN THICKNESS ON DYNAMIC TOUGHNESS

In the above discussion, the dynamic fracture initiation toughness, K_{IC}^d and the dynamic crack growth toughness K_{ID}, correspond to conditions of plane strain (specimens are thick enough that two-dimensional plane strain conditions dominate throughout the crack front). As the specimen thickness decreases, the critical values will eventually become dependent on the ratio of thickness to the plane strain plastic zone size, r_p, as first investigated by Irwin (1962) and described by Kanninen and Popelar (1985). The dependence of the static toughness K_c^s, on thickness is well-established. However, very little is known for the equivalent phenomenon for dynamic initiation or dynamic crack growth. Since this study is concerned with thin sheets of aluminum, the amplitudes of the right-hand sides of (3) and (5) should be replaced by the symbols K_c^d and K_D, respectively. These symbols denote the material fracture toughness of plates of arbitrary thickness, B, and they reduce to their plane strain values, K_{IC}^d and K_{ID} as $B/r_p \to \infty$. As a result, for through cracks in plates, the dynamic fracture initiation and growth criteria should read

$$K_I^d(P(t), a_0) = K_c^d(\dot{K}_I^d(t), B/r_p) \quad \text{at } t = t_o \tag{6}$$

and

$$K_I^d(P(t), a(t), \dot{a}(t)) = K_D(\dot{a}(t), B/r_p) \quad \text{for } t > t_o. \tag{7}$$
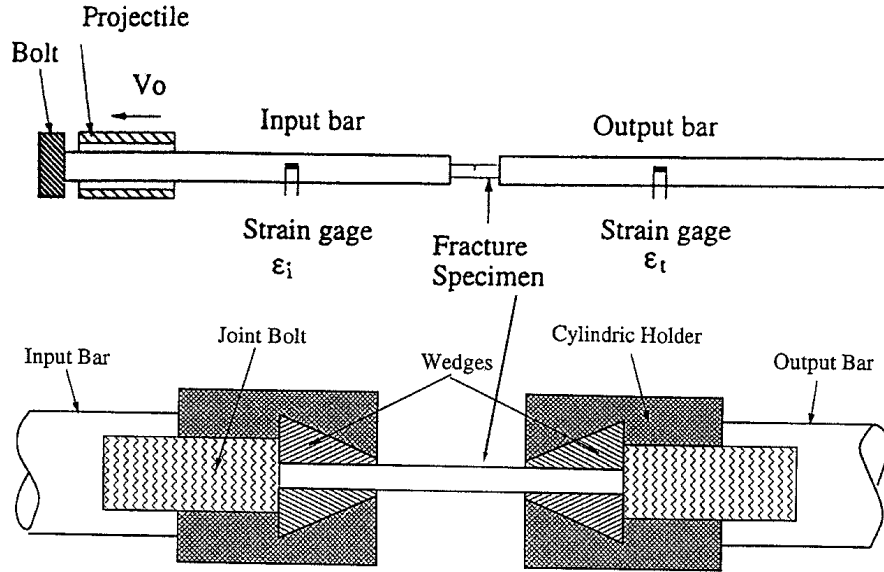
Figure 4. Schematic illustration of the split Hopkinson tension bar (SHTB) used to determine the dynamic initiation fraction toughness. A detail of the wedge gripping technique is shown below.

3. Dynamic crack initiation fracture toughness

3.1. EXPERIMENTAL

Thin sheets of 2024-T3 aluminum of 1.63, 2.03 and 2.54 mm in thickness were used in this investigation. Specimens of all three thicknesses with nominal planar dimensions of width, $w = 12.7$, and length, $l = 57$ mm were used to determine the initiation fracture toughness K_c^d. A notch 0.25 mm wide and 3.8 mm deep was cut using a wire EDM into the center of the 57 mm side of the specimen. Subsequently, the specimens were fatigued in a 3-point bend configuration in order to extend a sharp fatigue crack from the end of the notch. The length of the fatigue crack typically was $0.5-1$ mm, resulting in a total initial crack length, $a_o \sim 4.5$ mm such that $a_o/w \sim 0.35$. A schematic of the specimen geometry is shown in Figure 3.

The variation of K_c^d with loading rate, K_I^d was determined using hydraulic MTS load frame for $\dot{K}_I^d < 10^2 \, \mathrm{MPa\,m^{1/2}\,s^{-1}}$, and a split Hopkinson tension bar (SHTB) for $\dot{K}_I^d > 10^5 \, \mathrm{MPa\,m^{1/2}\,s^{-1}}$. A three-point bend configuration with a span, $S = 50$ mm, was used in the quasistatic MTS experiments. The variation of load with time was recorded continuously using a digital Nicolet oscilloscope. Following the experiment the value of a_o, was measured directly in an optical microscope and the variation of K_I^d with time was then calculated using the expression (Anderson, 1991)

$$K_I^d = \frac{P(t)}{B\sqrt{w}} \frac{3\frac{S}{w}\sqrt{\frac{a}{w}}}{2\left(1 + 2\frac{a}{w}\right)\left(1 - \frac{a}{w}\right)^{3/2}}$$

$$\times \left[1.99 - \frac{a}{w}\left(1 - \frac{a}{w}\right)\left\{2.15 - 3.93\left(\frac{a}{w}\right) + 2.7\left(\frac{a}{w}\right)^2\right\}\right], \tag{8}$$

where P is the load, B is the specimen thickness, and w is the specimen width. The loading rate $\dot{K}_I^d$ was calculated using a least squares fit to the linear portion of the loading curve. The

initiation fracture toughness was taken as the point where a line having a slope of 0.95 $\dot{K}_{\mathrm{I}}^{d}$ intersected the K_{I}^{d} versus time curve. In all experiments, the intersection occurred at a point to the left of the peak value of K_{I}^{d}.

Figure 4 shows the experimental configuration used in the SHTB to produce dynamic tensile loading. Four-angled steel tabs were attached to each side and at both ends of the specimens using a high strength adhesive (Loctite Speed Bonder 312). The tabs were positioned using a precision alignment fixture. The specimen was then placed in mating fixtures which were threaded into the end of each bar. A retaining ring was pressed around the assembly to constrain radial expansion of the fixture. In this manner, the specimen did not slip with respect to the steel tabs during the experiment.

Signals from strain gages mounted on both the input and output bars were recorded using a digital Nicolet oscilloscope. The magnitude of the transmitted signal provided the stress history in the specimen, $\sigma(t)$ from the following relation

$$\sigma(t) = \frac{A_b}{A_s} E_b \varepsilon_t(t), \tag{9}$$

where A_b and A_s are the cross-sectional areas of the bar and specimen, respectively, E_b is the Young's modulus of the bar and $\varepsilon_t(t)$ is the strain measured in the output bar. The tensile stress in the specimen was related to the value of $K_{\mathrm{I}}^{d}(t)$ by Anderson (1991)

$$
\begin{aligned}
K_{\mathrm{I}}^{d}(t) \;=\; & \frac{\sigma(t)w}{\sqrt{w}} \frac{\sqrt{2\tan\left(\frac{\pi a}{2w}\right)}}{\cos\frac{\pi a}{2w}} \\
& \times \left[0.752 + 2.02\left(\frac{a}{w}\right) + 0.37\left(1 - \sin\left(\frac{\pi a}{2w}\right)\right)^3 \right],
\end{aligned}
\tag{10}
$$

where the unconstrained specimen length l, was 12.7 mm. The loading rate $\dot{K}_{\mathrm{I}}^{d}$ and value of K_c^{d} was determined using the same approach described above for the quasistatic experiments.

It should be recognized that the validity of a static relation such as (10) for the determination of dynamic stress intensity factors by simply replacing the static stress with the history of the time varying load may be questionable unless certain conditions are satisfied. In particular, this assumption can be valid only if sufficient time has elapsed so that repeated wave fronts have traversed the specimen length enough times to establish quasi-equilibrium conditions. The necessary time should scale with l/c_l, where l is the maximum in-plane length scale of the specimen, and c_l ($c_l = \sqrt{E/\rho}$) is the dilatational (fastest) wave speed of the solid. Consequently, smaller specimens of stiffer materials will attain quasi-equilibrium faster than larger specimens of more compliant solids. It should be noted that the assumption of a quasi-equilibrium state is commonly made in the analysis of constitutive data obtained using the split Hopkinson bar, and it is expected to hold for fracture specimens as well. However, in the absence of a fully dynamic numerical or analytical solution, this assumption can be verified only through an independent experimental measurement, as described in the following section.

3.2. INDEPENDENT VERIFICATION OF BOUNDARY VALUE MEASUREMENT APPROACH

An evaluation of the validity of calculating the dynamic stress intensity factor based on time varying boundary load measurements is presented in this section. Experiments were conducted in which an independent local measurement of the stress intensity factor using the crack
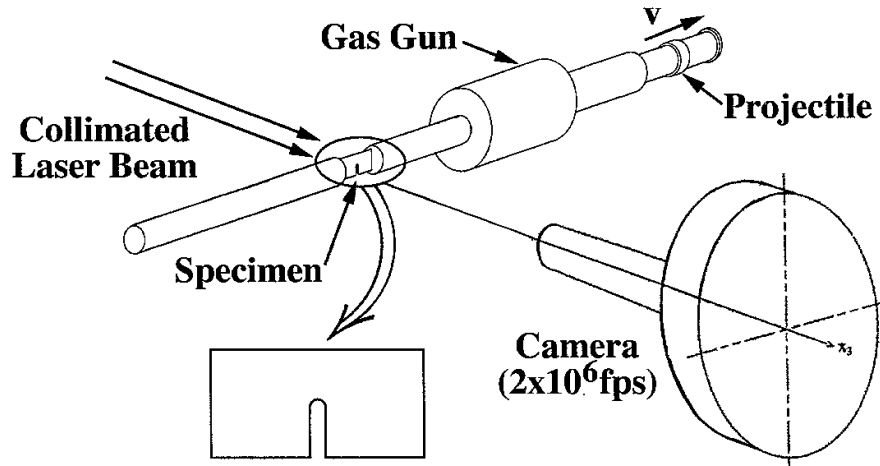
Figure 5. Schematic illustration of experimental configuration used to record high speed images of dynamic crack opening profiles.

opening displacement (COD) was compared to the values obtained from the boundary load history and (10). Real time images of the crack tip profile were obtained using high speed photography in a transmission arrangement providing a shadow image of the specimen as illustrated schematically in Figure 5. The SHTB and specimen were placed perpendicular to the path of a collimated laser beam 50 mm in diameter. The light passing through the specimen, which produced the shadow image of the specimen and a sharp, bright image of the notch and crack tip, was collected and focussed onto the film plane of a Cordin 330 high speed camera.

The thinnest sheet material ($t = 1.63$ mm) was used for the verification experiment in order to minimize any light loss due to slight misalignments or diffraction effects. A sharp crack was prefatigued from the end of a starter notch cut using a wire EDM. The camera recorded 80 frames with an interframe time of $2.1\,\mu$s. The resulting images were enlarged substantially to facilitate accurate measurements of the crack opening displacements. The value of the J-integral was evaluated using the relation given by Shih (1981)

$$\delta(r) = \alpha\varepsilon_o \left\{ \frac{J}{\alpha\sigma_o\varepsilon_o I_n} \right\}^{n/(n+1)} r^{n/(n+1)}[2\widetilde{u}_2(\pi, n)],\tag{11}$$

where $\delta(r)$ is the crack opening displacement at a distance r behind the crack tip. It is reasonable to assume that this relation is valid very near the stationary crack tip due to the existence of crack tip plasticity enveloping the area of measurement under conditions of small scale yielding. The parameters α and n are the constants associated with the Ramberg–Osgood description of material constitutive behavior, σ_o is the yield stress, ε_o is the reference strain ($\varepsilon_o = \sigma_o/E$, where E is the Young's modulus), I_n and $\widetilde{u}_2(\pi, n)$ are dimensionless functions dependent on the hardening exponent and stress state (plane stress or plane strain). If the crack tip opening displacement, δ_t, is measured at the intersection of two lines at 45° (with respect to the crack line) with the crack profile, (11) simplifies to

$$\delta_t = d_n(\varepsilon_o, \alpha, n)\frac{J}{\sigma_o},\tag{12}$$

Table 1. Relevant parameters of 2024-T3 aluminum for the evaluation of the J-integral from crack opening displacement measurements

Parameter	Value for 2024-T3 Al
α	0.87
hardening exponent, n	8.5
yield stress (MPa)	350.0
Young' modulus (GPa)	72.0

where the parameter d_n is a function of the reference strain, constitutive parameters and stress state. For small scale yielding conditions, the value of the J-integral is related to the stress intensity factor K_I by

$$J = \frac{K_I^2}{E}. \tag{13}$$

For the analysis of the current experiments, the parameters used for 2024-T3 aluminum are given in Table 1. The functions I_n, $\tilde{u}_2(\pi, n)$ and d_n have been tabulated by Shih (1983) and were evaluated for plane stress conditions. The time history of $J(t)$ was obtained by measuring $\delta(r)$ at a specific distance behind the crack tip or δ_t (at the 45° intercepts) and using (11) or (12), respectitvely. Relation (13) was then used to obtain $K_I^d(t)$.

Figure 6 shows a selected series of 10 such images, with time $t = 0$ corresponding to the onset of loading. Images were recorded with an interframe time of 2.1 μs such that the sequence shown in Figure 6 represents only half of the frames recorded over the time interval represented by the series. The crack profile is seen as the vertical bright regions. The first four images show only the pre-notch as it opens; the pre-fatigue crack has not yet opened sufficiently to let light pass through. For reference, the length of the initial notch is 3.76 mm. The opening of the pre-fatigue crack becomes visible in the images recorded at times greater than 16.8 μs. By $t = 21.0 \mu$s, the pre-fatigue crack has opened enough such that its entire length (4.32 mm) is visible. At times greater than 29.4 μs, extension of the pre-fatigue notch is apparent, signaling that dynamic crack initiation has occurred.

It should be recognized that the evidence for crack initiation from the images represents the latest time at which initiation may have occurred since it is possible that the crack may have propagated without having opened sufficiently to allow light to pass through. To determine the time of initiation as accurately as possible, the visible crack length was plotted as a function of time, as shown in Figure 7. Three distinct regimes are apparent in Figure 7. At short times, only the notch of length 3.76 mm is visible. At intermediate times the pre-fatigue crack can be seen and the visible crack length increases rapidly to the length of the initial crack length ($a_o = 4.32$ mm). After the crack has started propagating, the increase in visible crack length becomes more gradual. The intersection of the curves corresponding to the second and third regimes yields an approximate time of crack initiation at $t_i = 20 \pm 1 \mu$s. It is interesting to note that the initial crack velocity, inferred from the slope of the third regime, is only 17 m s^{-1}.

A comparison of the values of $K_I(t)$ calculated from the measured boundary loading history, (9 and 10), and crack opening displacement, (11–13), are shown in Figure 8. Crack
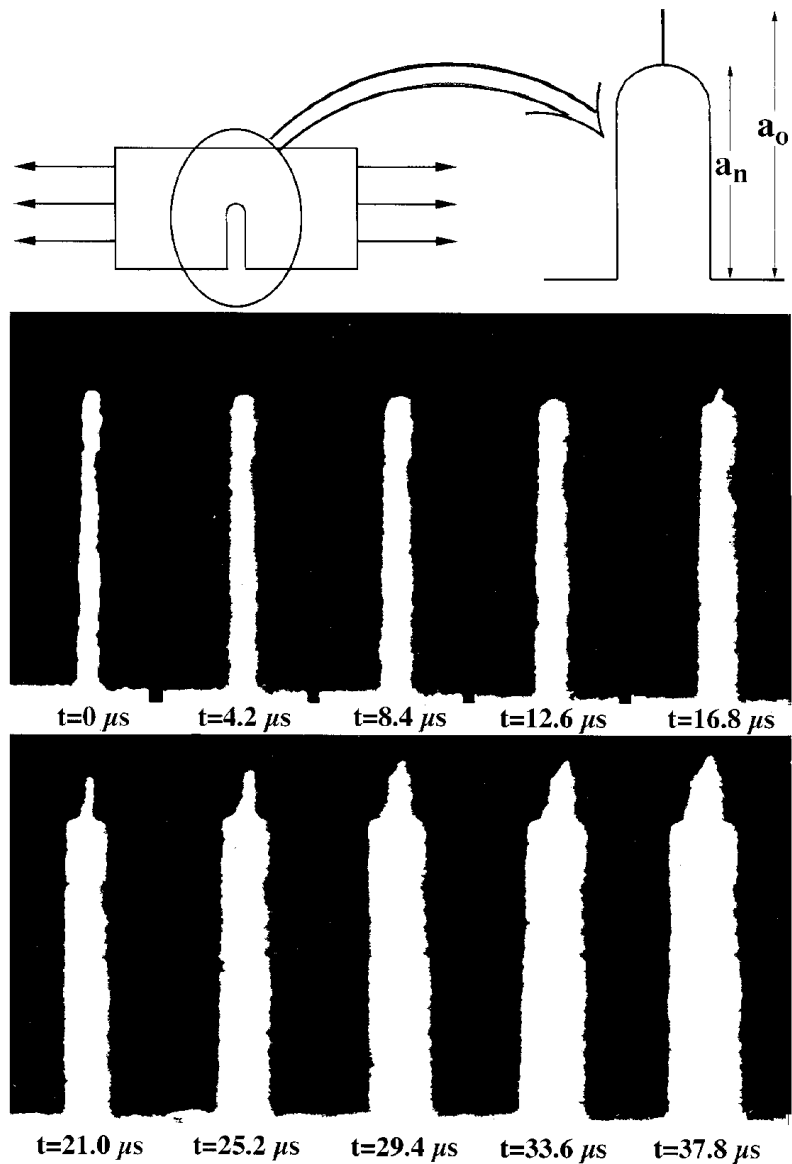
Figure 6. Selected sequence of high speed images of crack opening profiles in 2024-T3 aluminum. The length of the initial notch, a_n, and crack, a_o, were 3.76 and 4.32 mm, respectively.

opening displacement measurements were made at both the fatigue crack tip, shown as circles in Figure 8 and at the tip of the notch, shown as squares. The values based upon the measurements of the notch opening were calculated by taking the change in notch width, where the initial notch width was 0.30 mm, at a distance typically 0.7 mm behind the actual pre-fatigue crack tip. The open symbols in Figure 8 correspond to times after the initiation time inferred from Figure 7. The two types of measurements are correlated in time by shifting the signal measured by the transmitted gage by an amount equal to the distance of the gage from the specimen divided by the longitudinal wave speed of the bar ($c_l^b = 5000 \, \mathrm{m \, s^{-1}}$). The error bars shown on the symbols in Figure 8 correspond to uncertainties in a variety of delays associated
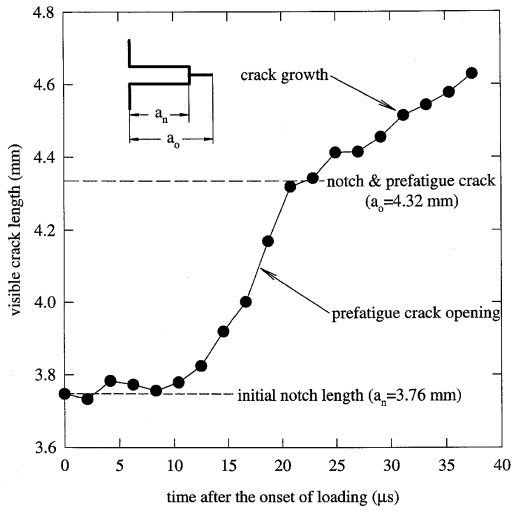
Figure 7. Variation of visible crack length with time measured from high speed images of the crack opening profile.
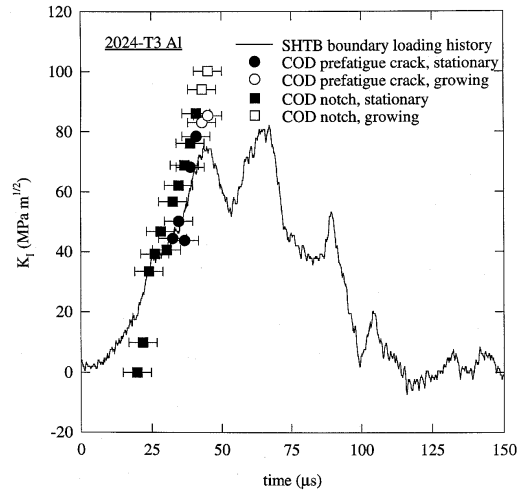

Figure 8. Comparison of the values of K_I determined from boundary loading history and crack opening displacement measurements.

with the high speed camera system as well as the uncertainty in estimating the wave travel time from the specimen to the gage. The errors in the calculated values of K_I are $\pm 2\,\mathrm{MPa\,m^{1/2}}$ which is approximately the size of the symbols in the vertical direction.

Inspection of Figure 8 reveals that there is very close agreement between the measurements at times greater than about $20\,\mu s$. At short times, it is expected that there should not be good agreement between the two measures since (9) is derived assuming that the specimen is in quasi-equilibrium. It has been demonstrated that equilibrium conditions are attained in the Hopkinson bar after the stress waves have traversed the specimen a minimum of three times. For an unclamped specimen length of $\sim 13\,\mathrm{mm}$, longitudinal waves in aluminum $(c_l^{Al} = 5000\,\mathrm{m\,s^{-1}})$ would traverse the distance of 78 mm necessary for three round trips in $\sim 16\,\mu s$. After the specimen has attained quasi-equilibrium, it is clear that there is good correlation between the two independent techniques. The values from the COD measurements, however are systematically higher than those calculated from the boundary load, and the COD values measured at the notch tip are slightly higher than those measured along the fatigue crack. Nevertheless, the value of K_c^d determined from the boundary load measurements was $74.5\,\mathrm{MPa\,m^{1/2}}$ whereas the corresponding values of K_c^d from the notch tip and crack tip COD measurements were 78.5 and $86.3\,\mathrm{MPa\,m^{1/2}}$, respectively. After initiation has occurred, the COD values continue to increase as the crack opens, whereas the boundary load values display a distinct decrease. In summary, it is apparent from the data presented in Figure 8 that the boundary loads measured with the SHTB can be used to calculate stress intensity factors, provided the specimen is sufficiently short such that equilibrium conditions are attained.

3.3. RESULTS

Figure 9 shows the variation of K_I^d with time for a quasistatic experiment for a specimen of $2.54\,\mathrm{mm}$ in thickness and a loading rate $\dot{K}_I^d = 1 \times 10^{-1}\,\mathrm{MPa\,m^{1/2}\,s^{-1}}$. In Figure 9 there is a regime of approximately linear variation of K_I^d with time for times between $150\,\mu s$ and
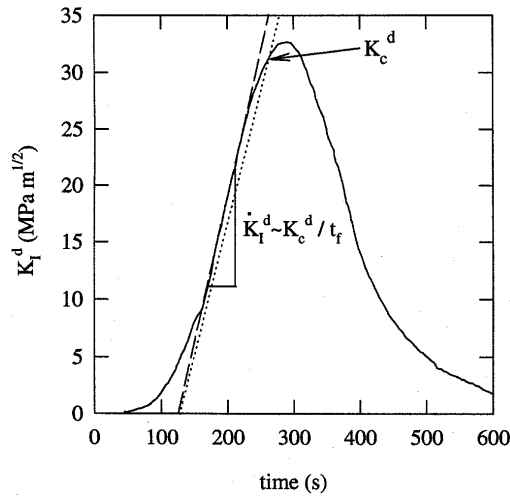
Figure 9. The variation of K_I^d with time for a quasistatic experiment conducted in 3-point bend. The determination of the loading rate and critical stress intensity factor are illustrated in the figure.
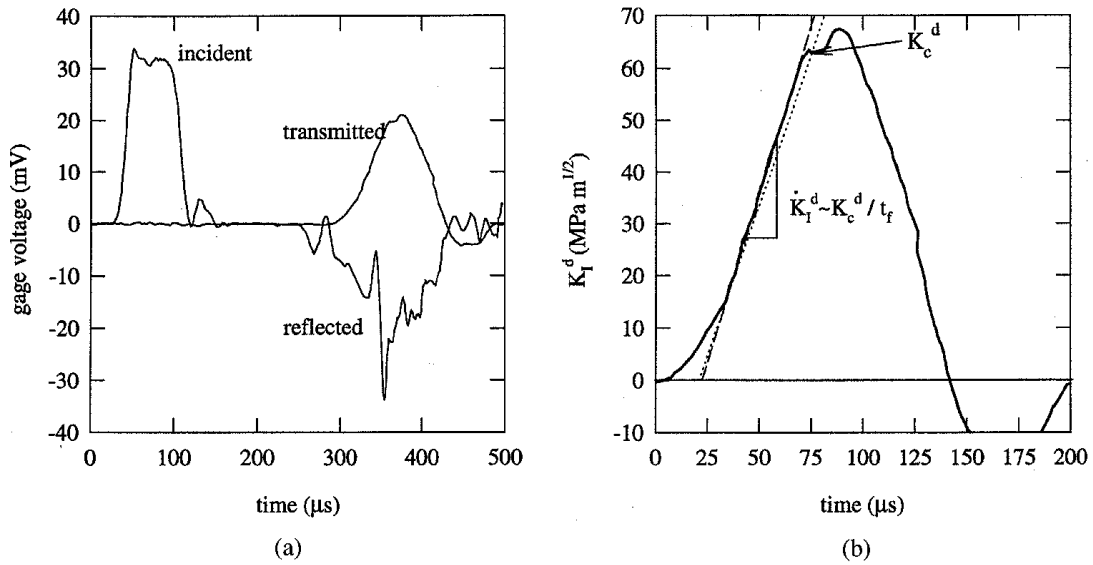

(a)

(b)

Figure 10. Results from a typical dynamic crack initiation experiment: (a) strain gage signals recorded from the SHTB showing the incident and reflected pulses (input bar) and the transmitted pulse (output bar), (b) determination of the critical dynamic stress intensity factor using the transmitted pulse and (9, 10).

$250\,\mu s$. The slope of this region was determined from a least squares fit, shown as a dashed line in the figure. The value of K_c^d is indicated on the experimental curve at the point of intersection with the dotted line having a slope of $0.95\dot{K}_i^d$ at a value of $K_c^d = 33\,\text{MPa}\,\text{m}^{1/2}$. It can be seen in Figure 9 that the intersection of the dotted line occurs to the left of the peak value of $K_I^d(t)$ and less than the maximum $K_I^d(t)$ by approximately 10 percent.
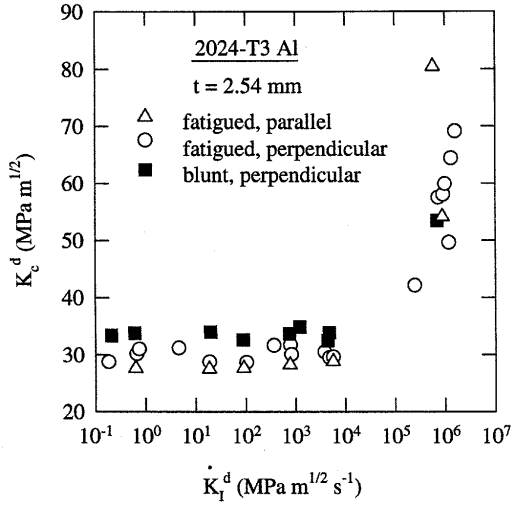
Figure 11. The variation of critical dynamic stress intensity factor with loading rate for specimens of 2.54 mm in thickness with different initial notch conditions.
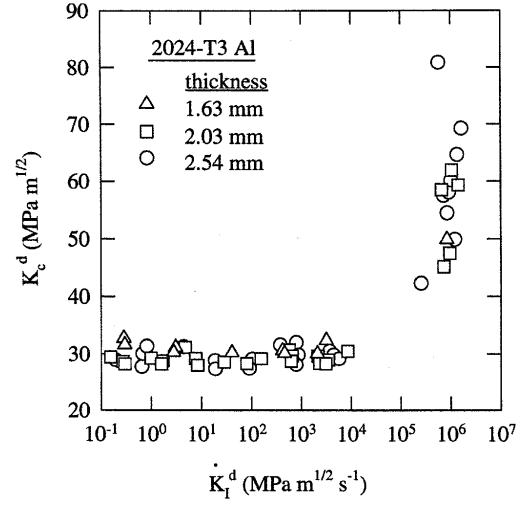
Figure 12. The variation of critical dynamic stress intensity factor with loading rate for specimens of each thickness.

Results from a typical dynamic crack initiation experiment conducted in the SHTB are shown in Figure 10 for a specimen having a thickness of 2.54 mm. Figure 10(a) shows the raw signals as a function of time: the solid line is the signal recorded from the strain gage on the input bar, whereas the dashed line is the signal recorded from the strain gage on the output bar. It should be noted that the transmitted signal shown in Figure 10(a) is amplified by a factor of 10. However, in spite of the relatively low transmitted signals, it is clear from Figure 10(a) that the signal to noise ratio was sufficiently high to allow for accurate determination of the value of K_c^d as illustrated in Figure 10(b). Figure 10(b) shows the variation of K_I^d with time for the dynamic experiment as calculated by using (9, 10) and the transmitted signal.

Similar to the approach described for the analysis of the quasistatic data shown in Figure 9, the loading rate $\dot{K}_I^d$ was determined by a least squares fit to the linear portion of the loading curve shown as a dashed line in Figure 10(b) and was determined as $1.4 \times 10^6\,\mathrm{MPa\,m^{1/2}\,s^{-1}}$. The value of K_c^d was then determined by the intersection of a line with slope $0.95\,\dot{K}_I^d$ with the $K_I^d(t)$ curve, which in this example occurred at $K_I^d = 64\,\mathrm{MPa\,m^{1/2}}$. Comparison of this value with the quasistatic limit obtained at low loading rates ($K_c^d \rightarrow K_c^s$ as $\dot{K}_I^d \rightarrow 0$) as shown in Figure 9, reveals an increase of a factor of ~ 2 as the loading rate increases by seven orders of magnitude.

The data obtained for K_c^d over seven orders of magnitude in loading rate is shown in Figure 11 for the 2.54 mm thick specimens. The results shown in Figure 11 are for specimens with the fatigue crack either perpendicular or parallel to the rolling direction. In addition, some specimens were tested which had a blunt EDM notch of radius $125\,\mu m$ perpendicular to the rolling direction. The type of initial flaw (pre-fatigued crack or blunt notch) and rolling direction are noted in the figure. Inspection of the figure reveals that essentially identical results were obtained for both crack orientations, whereas the measured K_c^d for blunt notch specimens were typically 5–10 percent higher than those having a fatigue crack. Under dynamic loading conditions, the values of K_c^d increased dramatically with loading rate. Indeed
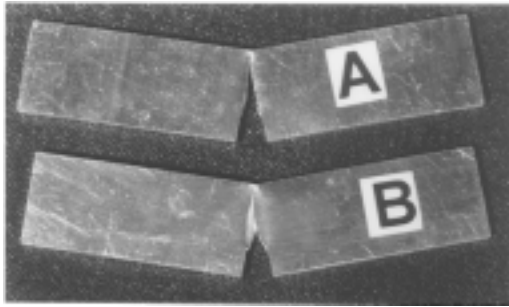
Figure 13. Fracture specimens with the initial notch cut (a) parallel to the rolling direction showing flat fracture and (b) perpendicular to the rolling direction showing slant fracture.
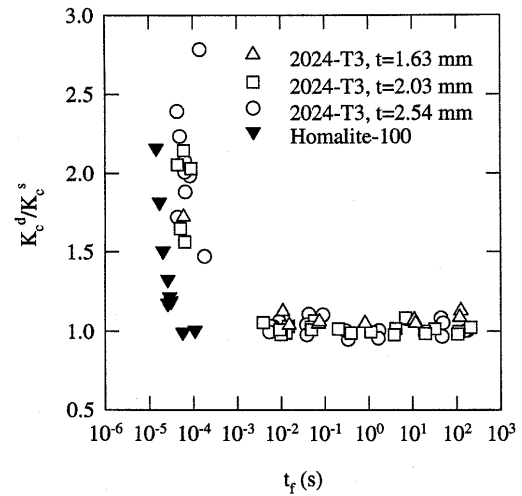

Figure 14. Normalized critical dynamic stress intensity factor versus time to failure. Plotted for comparison is data obtained on a brittle polymer, Homalite-100 (Ravi-Chandar and Knauss, 1984).

the variation suggests the existence of a vertical asymptote in K_c^d for loading rates in the vicinity of $10^7\,\mathrm{MPa\,m^{1/2}\,s^{-1}}$. Similar trends were observed in the results obtained on the specimens of 1.63 and 2.54 mm in thickness.

Figure 12 compares the results obtained from all three thickness, plotted as K_c^d versus $\dot{K}_I^d$. Several interesting features are apparent. First, within experimental scatter, the value of K_c^d is independent of thickness over the range of thickness tested ($1.63 < t < 2.54$ mm). Also K_c^d is independent of loading rate and has an average value of $30 \pm 3\,\mathrm{MPa\,m^{1/2}}$, for $\dot{K}_I^d <$ $10^4\,\mathrm{MPa\,m^{1/2}\,s^{-1}}$. This value is called the quasi-static fracture toughness K_c^s of the aluminum sheets. Its apparent independence of thickness is only due to the fact that a very small thickness range was tested in the present study. At loading rates greater than $10^4\,\mathrm{MPa\,m^{1/2}\,s^{-1}}$ there is a dramatic increase in the measured values of K_c^d with increasing $\dot{K}_I^d$. For example, data obtained when $\dot{K}_I^d = 2 \times 10^5\,\mathrm{MPa\,m^{1/2}\,s^{-1}}$ indicated $K_c^d = 46\,\mathrm{MPa\,m^{1/2}}$, whereas at the maximum loading rate achieved in the present study, $2 \times 10^6\,\mathrm{MPa\,m^{1/2}\,s^{-1}}$, $K_c^d = 77\,\mathrm{MPa\,m^{1/2}}$ which is ~ 2.5 times greater than the quasistatic value.

Examination of the fracture surfaces of specimens of each thickness revealed two distinct types of surfaces which are illustrated in Figure 13. In all of the specimens with the crack perpendicular to the rolling direction, the fracture surfaces were slanted at 45° to the specimen surface as shown in specimen *B* in Figure 13. Such fracture surfaces are typically observed in experiments on thin sheets where a state of plane stress dominates. Similar fracture surfaces were observed in many of the specimens tested with the crack parallel to the rolling direction. However in a limited number of these specimens, such as specimen *A* in Figure 13, the fracture surfaces were perpendicular to the specimen surface (i.e. flat fracture more typically observed under plane strain conditions).

Figure 14 shows the data from the present study plotted as K_c^d/K_c^s versus time to failure, t_f where t_f is defined by the relation $\dot{K}_I^d = K_c^d/t_f$. Also shown in Figure 14 are dynamic fracture toughness data obtained on Homalite-100 by Ravi-Chandar and Knauss (1984). The

two normalized data sets are shown in the same figure in order to compare directly the dynamic fracture initiation behavior of the ductile aluminum alloy with that of a relatively brittle polymer. Comparison of the two sets of data reveals that the qualitative behavior is very similar. Indeed, in both materials the dynamic fracture toughness increases drastically with decreasing time to fracture (increasing rate). The general shapes of each curve are surprisingly similar, indicating a minimum time necessary to initiate crack growth. However, the minimum recorded time to fracture in the brittle polymer is approximately $\frac{1}{3}$ of that observed in the ductile aluminum alloy.

In an attempt to understand some of the reasons for the observed increase of the dynamic fracture toughness with rate, Liu, Knauss, and Rosakis (1998) have analytically modelled the exact experimental configuration used by Ravi-Chandar and Knauss (1984) by means of a fully transient elastodynamic solution. They also modelled the decohesion process in the vicinity of the crack tip by introducing an array of favorably aligned microcracks within the fracture process zone. They considered that the closest of such microcracks (flaws) lies a distance δ away from the main crack tip and mandated that crack initiation will occur when this microcrack coalesces with the main crack. In this manner, they were able to study the rate dependence of this process by 'analytically' varying the loading rate through appropriate time variation of the dynamic boundary loads. It was demonstrated that the observed increase in K_c^d with rate was a consequence of the finite time necessary to achieve a critical stress state strong enough to initiate propagation of the flaw at δ. In other words, the effect was qualitatively predictable on the basis of purely 'elastodynamic' considerations (inertia only) without plasticity, rate sensitivity or adiabatic thermal effects being included in the model. This rather simplistic approach does indeed work well for brittle, nominally elastic solids, such as ceramics, glasses and some polymers, but should be modified for the case of structural metals.

In metals the interplay of inertia with plasticity, rate sensitivity and adiabatic heating strongly effects the mechanisms of ductile fracture initiation depending on both the constitutive and micromechanical characteristics of the metal. A general discussion of these phenomena is given in Chapter 3.6 of Freund (1990). Although mechanisms of ductile fracture initiation are associated with the nucleation, growth and coalescence of voids in the vicinity of the crack tip, an analogous phenomenon may result in the experimentally observed variation of K_c^d with t_f. Here again, there may be a finite time associated with attaining a critical stress or strain to nucleate a void at a given distance from the crack tip. Furthermore, sufficient time will be necessary in order for the void to grow to a critical size leading to failure in the ligament between the crack tip and void (i.e. crack initiation). Moreover, such a microseparation process is expected to be intimately connected with the rate of loading through the rate dependence of the flow stress (strain rate hardening) in the vicinity of the crack tip (Tong and Ravichandran, 1995). The above discussion implies that in structural materials such as aluminum alloys, steels, titanium alloys, etc. the dynamic fracture toughness may be affected by many additional mechanisms other than pure elastic inertia as observed in brittle polymers. This explains the fact that in Figure 14 the increases in dynamic fracture toughness is observed at lower loading rates in the aluminum alloy as compared to Homalite-100. However from a phenomenological 'macroscopic' viewpoint, the trends appear similar.
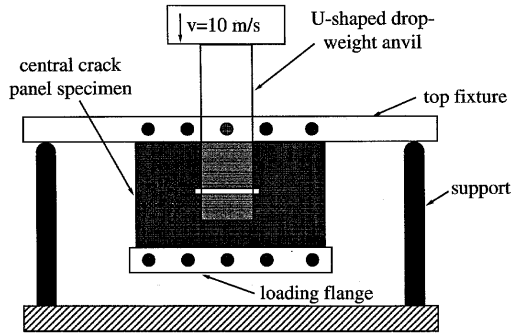
Figure 15. Schematic illustration of the dynamic tensile loading of a central crack panel used to characterize dynamic crack growth. A modified drop weight tower with a U-shaped anvil was used to impact a flange attached to the lower end of the specimen at a velocity of $10\,\mathrm{m\,s}^{-1}$.
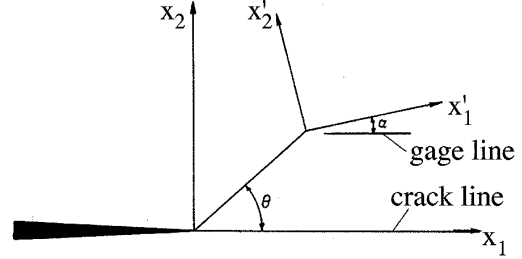

Figure 16. The coordinate system used in the analysis of crack propagation using strain gages (Dally and Berger, 1993).

4. Crack propagation toughness

4.1. EXPERIMENTAL

Specimens used for the determination of the variation of crack propagation fracture toughness K_D with crack tip speed were fabricated from larger panels. Central notch specimens $\sim 100\,\mathrm{mm}$ wide and $\sim 150\,\mathrm{mm}$ in length were fabricated from the 2.03 and 2.54 mm thick material. The central notch was 50 mm in length and $\sim 1.5\,\mathrm{mm}$ wide.

The central crack specimens were loaded in tension using a modified drop weight tower and fixture, as shown in Figure 15. The top end of the specimen was located between two 25 mm square steel bars using 5 pins which were secured with clamps, whereas two 25 mm thick and 100 mm wide steel flanges were attached to the bottom of the specimen. The top bars were supported on either side of the specimen, and a U-shaped anvil was attached to the drop weight hammer which symmetrically impacted the lower flanges to load the specimen in dynamic tension. In the figure, the U-shaped anvil is drawn semi-transparent to show the complete specimen shape. An impact velocity of $v_i = 10\,\mathrm{m\,s}^{-1}$ was used in all the experiments.

The propagation of the crack was monitored using a series of strain gages. The use of strain gages to measure the stress intensity factor has been pioneered by Dally and Berger (1993) who have also reviewed the method in detail. Figure 16 defines schematically the coordinate systems used for the analysis of the stress intensity factor using strain gages. The gage is located at polar coordinates r and θ in a coordinate system whose origin is at the crack tip with θ measured with respect to the crack line. The orientation of the strain gage with respect to the crack line is measured by an angle α; the strain measured by the gage ε_g is along the x_1 direction. The relationship between the gage position and orientation, stress intensity factor, and elastic constants of the material is given by Dally and Berger (1993)

$$2\mu\varepsilon_g = \frac{K_I}{\sqrt{2\pi r}}\left(k\cos\tfrac{1}{2}\theta - \tfrac{1}{2}\sin\theta\sin\frac{3\theta}{2}\cos 2\alpha + \tfrac{1}{2}\sin\theta\cos\frac{3\theta}{2}\sin 2\alpha\right). \tag{14}$$

The constants μ and k are dependent on Young's modulus and Poissons ratio through $2\mu = E/(1+\nu)$ and $k = (1-\nu)/(1+\nu)$.
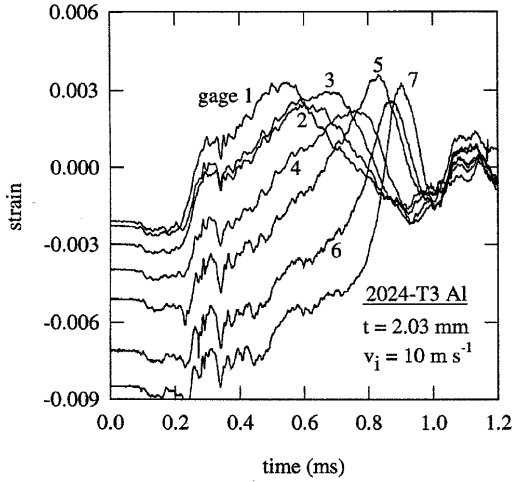
Figure 17. Strain measured from successive gages on a central crack panel specimen.
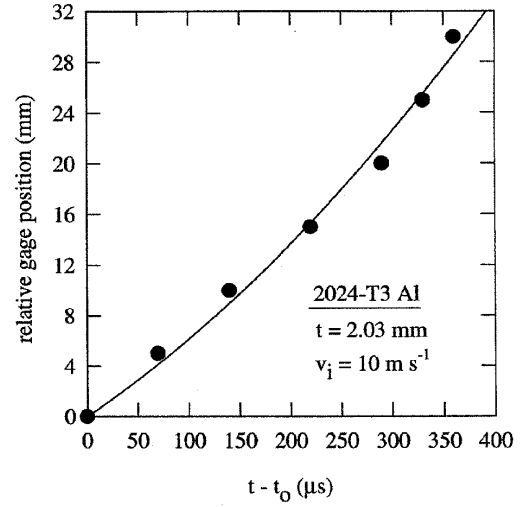

Figure 18. Variation of crack tip position with time from the data shown in Figure 17.

Equation (14) can be simplified if the appropriate angular orientations θ and α are selected for a material of a given Poisson's ratio. In the case of aluminum with $\nu = 0.33$, the selection of $\theta = \alpha = 60°$ reduces (14) to

$$K_{\mathrm{I}} = E\sqrt{\frac{8}{3}\pi r}\varepsilon_g. \tag{15}$$

Equations (14) and (15) were developed based upon a static analysis of the crack tip fields. They are expected to be valid for analysis of the current experiments where, as shown below, the crack speeds were less than 5 percent of the shear wave speed and, as a result, dynamic effects were negligible. In the present experiments, 350 ohm strain gages were positioned along a line parallel to the crack path at a distance of 11 mm. Each gage was oriented at an angle of 60° with respect to the axis of the initial notch. The strain gage signals (up to seven) were recorded using two Nicolet digital oscilloscopes.

From (14), it can be shown that for a given value of K_{I}, the maximum strain measured for each strain gage signal corresponds to the time when the axis of the gage (oriented at 60° to the notch axis) was intersected by the moving crack. In this manner, the position of the crack with time could be determined from the measured relative positions of the gages and time between the peaks in the signals from successive strain gages. The value of K_D was then calculated using (15) and the crack velocities were determined by the differentiation of a plot of crack position versus time.

4.2. RESULTS

Figure 17 shows the signals obtained from seven strain gages mounted on a 2.03 mm thick central crack panel loaded in tension at an impact velocity of 10 m s^{-1}. In the figure the gage signals are numbered 1 to 7 to indicate the relative position of each gage with respect to the initial notch tip with 1 being closet and 7 being furthest. In Figure 17, a significant increase in strain is observed as the axis of the gage intersects the crack path for the successive gages.
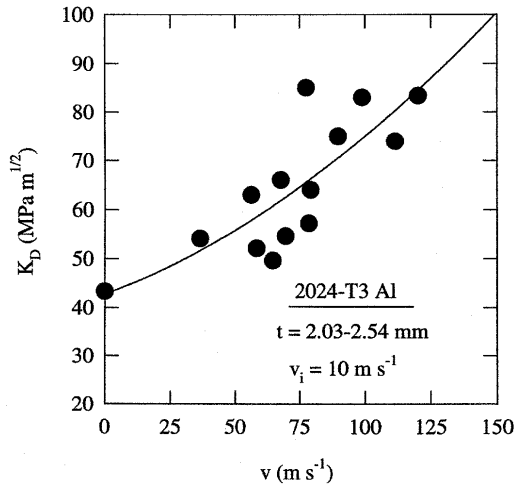
Figure 19. The variation of dynamic crack propagation toughness with crack tip speed.
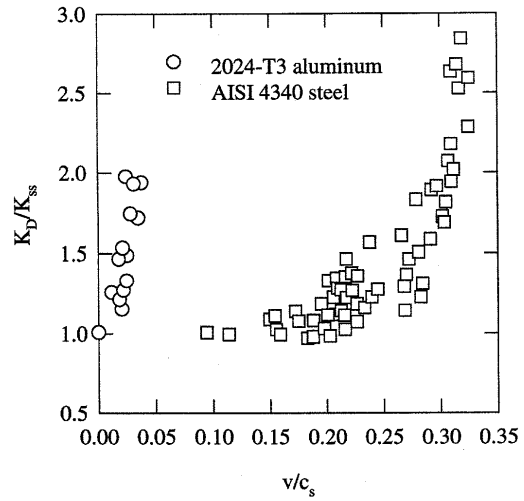

Figure 20. Normalized dynamic crack propagation toughness versus normalized crack tip speed. Shown for comparison is data for AISI 4340 high strength steel (Zehnder and Rosakis, 1990).

Also apparent in Figure 17 are the increasingly narrow strain peaks for higher gage numbers, which can be attributed to an increase in crack velocity as the crack approaches the edge of the panel. Since the earlier peaks are somewhat broad, it is more difficult to accurately determine the crack position and hence there is slightly more error associated with measuring slower crack speeds.

Figure 18 shows the variation of crack tip position with time using the data presented in Figure 17. A position of 0 and time $t_o = 0$ in Figure 18 corresponds to the position of gage 1 and the time at which peak signal from gage 1 was recorded, respectively. The increase in the slope of the position-time plot indicates the increase in crack velocity with time.

The values of stress intensity factors and velocities determined from data of the type shown in Figures 17 and 18 are summarized in Figure 19. The data shown in Figure 19 include data obtained using material of both 2.03 and 2.54 mm in thickness. Although there is scatter amongst the data in Figure 19, a general trend of increasing K_D with crack velocity is apparent. For example, at the highest velocity ($v \sim 125\,\mathrm{m\,s^{-1}}$) a value of $K_D = 85\,\mathrm{MPa\,m^{1/2}}$ was measured, which is approximately twice that measured for slowly growing cracks $K_{ss} = 43\,\mathrm{MPa\,m^{1/2}}$. It should be recognized that K_{ss} is not equal to the quasistatic initiation toughness for a ductile metal. Instead it is the value of the toughness of a quasistatically growing crack at a very low speed. The quasistatic initiation toughness K_c^s is typically lower than K_{ss} which is the plateau value of the so-called K-resistance curve of the material. For brittle solids, K_c and K_{ss} coincide.

A similar increasing trend in dynamic crack growth toughness was observed by Rosakis, Duffy and Freund (1984) and Zehnder and Rosakis (1990) in their study of AISI 4340 steel. Figure 20 compares the data from that study with the results from the present study where K_D is normalized by the steady state crack growth toughness K_{ss} and the velocity is normalized by the shear wave speed in the respective materials, c_s ($c_s^{Al} = 3100\,\mathrm{m\,s^{-1}}$; $c_s^{St} = 3190\,\mathrm{m\,s^{-1}}$).

When plotted in this manner, the differences between the two materials are striking. In both cases, the increase in toughness with crack speed implies the presence of a limiting velocity for crack propagation. However, in the steel this value is approximately $\frac{1}{3}$ the shear wave speed or $\sim 1000\,\mathrm{m\,s^{-1}}$, whereas for the 2024-T3 aluminum the limiting speed appears to be less than $0.05c_s$ or $\sim 155\,\mathrm{m\,s^{-1}}$, as indicated in the figure. The most probable reasons for such a pronounced difference are associated with differences in both the ductility and plate thickness. The 4340 steel tested by Zehnder and Rosakis (1990) is a martensitic high strength steel of yield stress $\sigma_o^{\mathrm{St}} \sim 900\,\mathrm{MPa}$ and the experiments were conducted using 10 mm thick plates under conditions approximating plane strain. However, the 2024-T3 aluminum alloy has a comparatively low yield stress, $\sigma_o^{\mathrm{Al}} \sim 350\,\mathrm{MPa}$ and the fracture experiments were conducted in thin sheets (1.5–2.5 mm in thickness) under nominally plane stress conditions.

As discussed by Freund and co-workers (Freund and Douglas, 1982, Lam and Freund, 1985 and Freund, 1990), for plane strain the dynamic fracture toughness of a rate insensitive metallic solid is expected to rise sharply at a specific normalized crack tip speed (terminal speed). This critical speed decreases with increasing material ductility. A very similar trend is observed for plane stress crack growth considered by Deng and Rosakis (1991, 1992a, 1992b). However in the case of plane stress the terminal velocities are less than those for plane strain for materials of identical ductility. Indeed the results of Figure 19 are consistent with all of the above observations, since both higher ductility and lower thickness result in lower terminal speeds. As a result, it is expected that aluminum specimens of greater thickness will exhibit substantially greater terminal speeds than those observed in the present experiments on thin sheets.

Acknowledgements

References

Anderson, T.L. (1991). *Fracture Mechanics*, CRC Press, Boston.

Barnes, J. and Peters, R.L. (1992). The challenge of commercial aircraft survivability. In *Aerospace America* pp. 55–56.

Dally, J.W. (1979). Dynamic photoelastic studies of fracture. *Experimental Mechanics* **19**, 349–367.

Dally, J.W. and Berger, J.R. (1993). The role electrical resistance strain gages in fracture research. In *Experimental Techniques in Fracture* (Edited by J.S. Epstein), VCH Publishers, Inc., New York, 1–39.

Deng, X. and Rosakis, A.J. (1991). Dynamic crack propagation in elastic-perfectly plastic solids under plane stress conditions. *Journal of the Mechanics and Physics of Solids* **39**, 683–722.

Deng, X. and Rosakis, A.J. (1992a). A finite element investigation of quasi-static and dynamic asymptotic crack tip fields in hardening elastic–plastic solids under plane stress – I. Crack growth in linear hardening materials. *International Journal of Fracture* **57**, 291–308.

Deng, X. and Rosakis, A.J. (1992b). A finite element investigation of quasi-static and dynamic asymptotic crack tip fields in hardening elastic–plastic solids under plane stress – II. Crack growth in power-law hardening materials. *International Journal of Fracture* **58**, 137–156.

Freund, L.B. and Clifton, R. (1974). On the uniqueness of plane elastodynamic solutions for running cracks. *Journal of Elasticity* **4**, 293–299.

Freund, L.B. and Douglas, A.S. (1982). The influence of inertia on elastic–plastic antiplane shear crack growth. *Journal of the Mechanics and Physics of Solids* **30**, 59–74.

Freund, L.B., Duffy, J. and Rosakis, A.J. (1981). Dynamic fracture initiation in metals and preliminary results on the method of caustics for crack propagation measurements. ASME Paper No. 81-PVP-15.

Freund, L.B. (1990). *Dynamic Fracture Mechanics*, Cambridge University Press.

Irwin, G.R. (1962). Crack extension force for a part-through crack in a plate. *Journal of Applied Mechanics* **29**, 651–654.

Kamoulakos, A., Chen, V.L., Mestreau, E. and Lohner, R. (1996). Finite element modelling of structure/fluid interaction in explosively loaded aircraft fuselage panels using pamshock/pamflow coupling. Presented at the Conference on Spacecraft Structures, Materials and Mechanical Testing, ESA/CNES/DARA, Noordwijk, The Netherlands.

Kanninen, M.F. and Popelar, C.H. (1985). *Advanced Fracture Mechanics*, Oxford University Press, New York.

Kanninen, M.F. and O'Donoghue, P.E. (1995). Research challenges arising from current and potential applications of dynamic fracture mechanics to the integrity of engineering structures. *International Journal of Solids and Structures* **32**, 2423–2445.

Kosai, M. and Kobayashi, A.S. (1991). Axial crack propagation and arrest in pressurized fuselage. In *Structural Integrity of Aging Airplanes* (Edited by S.N. Atluri, S.G. Sampath and P. Tong) Springer-Verlag, Berlin, 225–239.

Kosai, M., Shimamoto, A., Yu, C.-T., Kobayashi, A.S. and Tan, P. (1996). A biaxial test specimen for crack arrest studies. *Experimental Mechanics* **36**, 277–283.

Lam, P.S. and Freund, L.B. (1985). Analysis of dynamic growth of a tensile crack in an elastic–plastic material. *Journal of the Mechanics and Physics of Solids* **33**, 153–167.

Liu, C., Knauss, W.G. and Rosakis, A.J. (1998). Loading rates and the dynamic initiation toughness in brittle solids, this issue, pp. 103–118.

Maigre, H. and Rittel, D. (1995). Dynamic fracture detection using the force-displacement reciprocity: application to the compact compression specimen. *International Journal of Fracture* **73**, 67–79.

Meyers, M.A. (1994). *Dynamic Behavior of Materials*, John Wiley and Sons, New York.

Ravi-Chandar, K. and Knauss, W.G. (1984). An experimental investigation into dynamic fracture: (i) crack initiation and arrest. *International Journal of Fracture* **25**, 247–262.

Rittel, D. and Maigre, H. (1996a). A study of mixed-mode dynamic crack initiation in PMMA. *Mechanics Research Communications* **23**, 475–481.

Rittel, D. and Maigre, H. (1996b). An investigation of dynamic crack initiation in PMMA. *Mechanics of Materials* **23**, 229–239.

Rosakis, A.J., Duffy, J. and Freund, L.B. (1984). The determination of the dynamic fracture toughness of AISI 4340 steel by the shadow spot method. *Journal of the Mechanics and Physics of Solids* **34**, 443–460.

Shih, C.F. (1981). Relationships between the J-integral and the crack opening displacement for stationary and extending cracks. *Journal of the Mechanics and Physics of Solids* **29**, 305–326.

Shih, C.F. (1983). Tables of Hutchinson–Rice–Rosengren singular field quantities.

Shimamoto, A., Kosai, M. and Kobayashi, A.S. (1994). Crack arrest at a tear strap under mixed mode loading. *Engineering Fracture Mechanics* **47**, 59–74.

Tong, W. and Ravichandran, G. (1995). Inertia effects on void growth in viscoplastic materials. *Journal of Applied Mechanics* **62**, 633–639.

U.K. Accidents Investigation Branch, (1990). Report on the accident to Boeing 747-121-W739PA at Lockerbie, Dumfriesshire, Scotland on 21 December 1988. Aircraft Accident Report 2/90, HMSO, London.

Wilson, M.L., Hawley, R.H. and Duffy, J. (1980). The effect of loading rate and temperature on fracture initiation in 1020 hot-rolled steel. *Engineering Fracture Mechanics* **13**, 371–385.

Zehnder, A.T. and Rosakis, A.J. (1990). Dynamic fracture initiation and propagation in 4340 steel under impact loading. *International Journal of Fracture* **43**, 271–285.